Mathematical modeling of chemotaxis and glial scarring around implanted electrodes



2015 New J. Phys. 17 023009

(http://iopscience.iop.org/1367-2630/17/2/023009)

IOP Publishing New J. Phys. 17 (2015) 023009 doi:10.1088/1367-2630/17/2/023009

New Journal of Physics
The open access journal at the forefront of physics

Deutsche Physikalische Gesellschaft DPG
IOP Institute of Physics

Published in partnership with: Deutsche Physikalische Gesellschaft and the Institute of Physics

OPEN ACCESS

RECEIVED
23 June 2014

REVISED
20 October 2014

ACCEPTED FOR PUBLICATION
31 December 2014

PUBLISHED
30 January 2015



PAPER

# Mathematical modeling of chemotaxis and glial scarring around implanted electrodes

**Alexander N Silchenko**[1] **and Peter A Tass**[1,2,3]

[1] Institute of Neuroscience and Medicine 7—Neuromodulation, Research Center Juelich, D-52425, Juelich, Germany
[2] Department of Neuromodulation, University of Cologne, D-50924 Cologne, Germany
[3] Department of Neurosurgery, Stanford University, Stanford, CA, USA

**E-mail:** a.silchenko@fz-juelich.de

**Keywords:** microglia chemotaxis, purinergic feedback, modeling, anti-inflammatory coating

## Abstract

It is well known that the implantation of electrodes for deep brain stimulation or microelectrode probes for the recording of neuronal activity is always accompanied by the response of the brain's immune system leading to the formation of a glial scar around the implantation sites. The implantation of electrodes causes massive release of adenosine-5′-triphosphate (ATP) and different cytokines into the extracellular space and activates the microglia. The released ATP and the products of its hydrolysis, such as ADP and adenosine, become the main elements mediating chemotactic sensitivity and motility of microglial cells via subsequent activation of $P2Y_{2,12}$ as well as A3A/A2A adenosine receptors. The size and density of an insulating sheath around the electrode, formed by microglial cells, are important criteria for the optimization of the signal-to-noise ratio during microelectrode recordings or parameters of electrical current delivered to the brain tissue. Here, we study a purinergic signaling pathway underlying the chemotactic motion of microglia towards implanted electrodes as well as the possible impact of an anti-inflammatory coating consisting of the interleukin-1 receptor antagonist. We present a model describing the formation of a stable aggregate around the electrode due to the joint chemo-attractive action of ATP and ADP and the mixed influence of extracellular adenosine. The bioactive coating is modeled as a source of chemo-repellent located near the electrode surface. The obtained analytical and numerical results allowed us to reveal the dependences of size and spatial location of the insulating sheath on the amount of released ATP and estimate the impact of immune suppressive coating on the scarring process.

## 1. Introduction

Nowadays, implantation of electrodes for deep brain recording of neuronal signals and electrical deep brain stimulation (DBS) are widely used for the therapy of several neurologic disorders [2–4, 1]. In addition, increasing evidence suggests that implantable electrode technology, including multielectrode arrays (MEA), may be applied in the context of brain–machine interface [5–7]. However, recent studies reported a decrease in the quality of neuronal signals and the number of functional electrodes in chronic MEA recordings caused by the brain's immune response [8, 9]. The *in vivo* response to the implantation of an electrode can be divided into the initial acute response to the cell damage and chronic response resulting in a formation of the electrode–tissue interface around the implantation site [8, 10]. Several clinically used DBS devices use voltage-controlled stimulation, which leads to a strong dependence of the injected current on the impedance of the electrode–tissue interface, which separates electrodes from the surrounding brain tissue [14, 16]. The impedance of the layer forming this interface increases with time, which in some cases makes it necessary to substantially increase the amplitude and/or frequency of the stimulation signal [18]. As follows from the immunohistochemical analysis, the main cellular components of the electrode–tissue interface are the microglial cells and reactive astrocytes [9]. Microglia are clustered around the implant in a reactive tissue sheath and persist throughout the whole lifetime

of the implant [10, 11]. The reactive astrocytes surround this inner core of microglia in an encapsulation layer referred to as the glial scar [8–10]. Thus, the glial scar encapsulates the electrode, creating a physical barrier between the electrode and the neurons that, in turn, defines a time limit for chronic recordings and stimulation [9, 1]. The results of *in vitro* and *in vivo* impedance spectroscopy together with the results of recent theoretical studies have shown that the resistivity of the encapsulation tissue is sufficient to alter the shape and magnitude of the electric field generated by chronically implanted electrodes [12, 15, 16, 21, 22].

The mechanism of the glial scar development is still not completely understood. Recent *in vitro* studies have shown that implanted electrodes cause chronic, local inflammation that is correlated with local neurodegeneration [13]. Indeed, the electrode's implantation initiates immune response, which is accompanied by a massive release of ATP and different immune response regulation factors such as tumor growth factor and pro-inflammatory cytokines [19, 20]. The strength of the immune response is tightly related to the level of extracellular ATP, as clearly demonstrated via the reduction of the inflammatory response by means of an inhibition of the P2X(7) receptor [23], which is the key player in processing and release of pro-inflammatory cytokines, such as interleukin (IL)-1 [24]. Moreover, ATP plays the role of a chemo-attractant, providing a clear 'navigation signal' for macrophages [25]. The implantation of electrodes as well as electrical stimulation induce a massive release of ATP from the injured cells [26], thus initiating a chemotactic response of microglia, which move towards the electrodes along the gradient of ATP concentration [25, 28, 29]. The formation of a glial scar around the electrode is a long-term process [8, 10], which is accompanied by the release of ATP and pro-inflammatory cytokines like IL-1 [20] as well as others gliotransmitters [30–32]. Some of the recently proposed strategies for improving the brain–electrode interface utilize the so-called 'passive' coating of electrodes by laminin [47, 48] as well as the anti-inflammatory coating by proteins of the IL-1 receptor antagonist (IL-1 ra) [49]. The nanoscale laminin coating has a stimulatory effect on early microglia activation and might potentially improve chronic neural recordings through the dispersion of the glial scar [48]. The main goal of the strategy utilizing the bioactive coating by proteins of IL-1 ra is to weaken the immune response and limit the area around electrode where the scarring processes are observed [49].

Recent experimental studies of microglia chemotaxis revealed the crucial role of purinergic receptors and ectonucleotidase cd39/ENTPDase1 and ecto-5′-nucleotidase/cd73 that degrade nucleotides to nucleosides, including adenosine [35]. In particular, ADP, AMP and adenosine, being products of ATP hydrolysis, play contrasting roles in the chemotactic signaling of microglia [25, 27, 29]. The extracellular ATP and ADP activate the purinergic $P2X_4$ and $G_i$-coupled $P2Y_{2,12}$ receptors and act as chemo-attractants [33, 36], whereas adenosine, initially functioning in concert with $P2Y_{2,12}$ via an activation of $G_i$-coupled A3A receptors, later on acts as a chemo-repellent via the stimulation of adenosine $G_s$-coupled A2A receptors what causes retractions of microglia [34, 37]. Thus, the co-stimulation of purinergic and adenosine receptors is the requirement for the microglia migration and expression of cd39 and cd73 to control the ATP/adenosine balance [27, 35, 37, 38]. The main reaction steps forming the autocrine purinergic feedback loop are schematically presented in figure 1. Apparently, to explore the mechanism of acute response and glial scarring one has to model the chemotactic motion of microglia towards the electrode, which is mantained by the autocrine purinergic feedback and results in the formation of the 'front line' consisting of the microglia cells due glued to the electrode's surface [9]. To model the impact of bioactive coating on the scarring process, one has to additionally incorporate a source of IL-1 ra into the model.

The first and most famous continuous mathematical model for chemotaxis was proposed more than forty years ago by Keller and Segel [39]. Since then, the Keller–Segel model has become one of the standard models in mathematical biology and is often used in situations when a simple continuous macroscopic model of an aggregation process is required, which also takes into account some features of the microscopic dynamics [40]. Numerous modifications of the classical Keller–Segel model were developed to take into account important features of real systems, such as receptors' dynamics and the effect of cells' overcrowding [40, 41]. The computational modeling of chemotactic signaling and motility of macrophages is of particular interest due to the important role they play in the inflammatory response [42]. The mathematical models of acute inflammatory processes usually describe the chemotactic response of macrophages to pro- and anti-inflammatory cytokines released by these cells [43, 44]. However, there is growing evidence for the key role played by ATP and the products of its hydrolysis in the extracellular space (ECS) [27, 33, 35, 45]. Moreover, it was observed that deletion of cd39 leads to a drastic decrease of the accumulation of microglia [35], underlying the crucial role of autocrine purinergic feedback loops for macrophage chemotaxis [25]. Apparently, the role of ATP as well as products of its degradation in the immune response during DBS is of special interest and importance because of the massive release of ATP during electrode implantation and electrical stimulation [26].

The objective of the present study is to model the chemotactic signaling and the aggregation of microglia in the presence of the stationary gradients of ATP, ADP and adenosine during the acute response caused by an electrode implantation. We present a simple continuous Keller–Segel based model, which describes dynamics of the microglia cells density and allows us to estimate the dependences of size and location of the insulating sheath

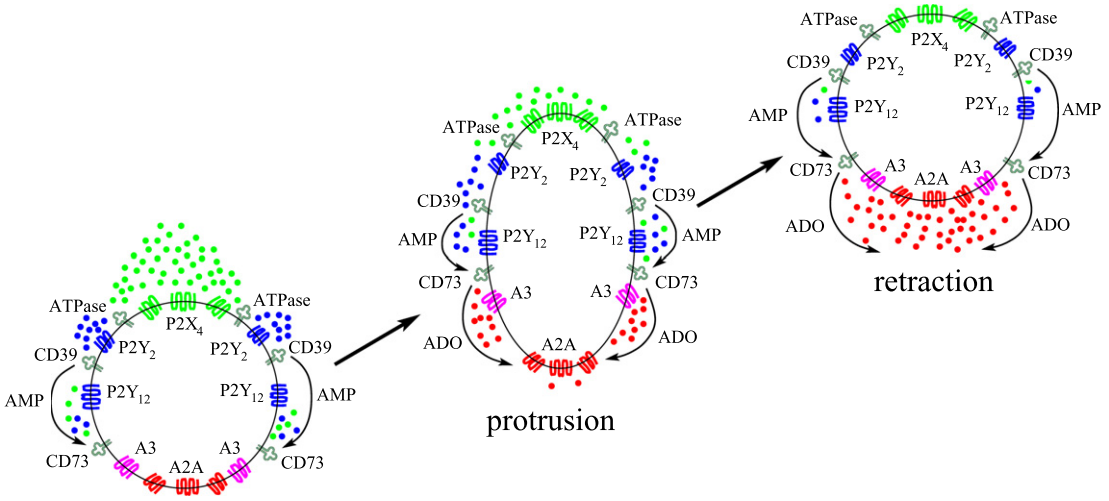


**Figure 1.** Schematic picture illustrating the main stages of the autocrine purinergic feedback loop involved in chemotaxis of microglia. At the first stage, ATP released from the damaged cells (green filled circles) activates $P2X_{4,7}$ receptors and evokes an ATP-induced release of ATP from microglial cells [51] and thus results in an activation of $P2Y_{2,12}$ receptors, which provides signal amplification and facilitates the sensing of the shadow chemotactic gradients [27]. The second stage is characterized by the polarization of the cells within the chemotactic gradient field and autocrine activation of A3A receptors by adenosine formed from AMP by ecto-5′-nucleotidase (CD73). At the last stage, adenosine (red filled circules) activates A2A receptors which causes retraction of the microglial cells and their movement towards the gradient of ATP.

on the amount of ATP released into the ECS. Apart from that, the impact of bioactive coating consisting of the IL-1 ra proteins on the glial scarring process is also taken into account in our model. The model of the glial scarring process is introduced in section 2. The analytical results for the linearized dimensionless equations are presented in section 3. In section 4, we analyzed the impact of the anti-inflammatory bioactive coating by means of stability theory. The results of numerical simulations for the two-dimensional case are presented in section 5. Our conclusions are given in section 6.

## 2. Model of microglial chemotactic acute response

The proposed macroscopic model of microglia chemotaxis is governed by the following equations:

$$
\begin{aligned}
\frac{\partial n}{\partial t} &= D_1 \Delta\, n - \nabla\left( \underbrace{\frac{n\,\chi_1}{\left(q^s_{\mathrm{atp}} + y_1\right)^2}\,\nabla y_1}_{\text{ATP gradient}} + \underbrace{\frac{n\,\chi_2}{\left(q^s_{\mathrm{adp}} + y_2\right)^2}\,\nabla y_2}_{\text{ADP gradient}} + n\,\chi_3\,\theta(y_4)\,\nabla y_4 - n\chi_4\,\nabla y_5 \right),\\
\frac{\partial y_1}{\partial t} &= D_2 \Delta\, y_1 + a\, n + \underbrace{b\, y_1/\left(y_1 + k_b\right)}_{\text{ATP release}} - \underbrace{v_1\, y_1/\left(y_1 + k_1\right)}_{\text{ATP}\to\text{ADP}} - \underbrace{w_1\, y_1/\left(y_1 + k_5\right)}_{\text{ATP}\to\text{AMP via cd39}},\\
\frac{\partial y_2}{\partial t} &= D_3 \Delta\, y_2 + v_1\, y_1/\left(y_1 + k_1\right) - \underbrace{v_2\, y_2/\left(y_2 + k_2\right)}_{\text{ADP}\to\text{AMP}},\\
\frac{\partial y_3}{\partial t} &= D_4 \Delta\, y_3 + v_2\, y_2/\left(y_2 + k_2\right) + w_1\, y_1/\left(y_1 + k_5\right) - \underbrace{v_3\, y_3/\left(y_3 + k_3\left(1 + y_2/k_i\right)\right)}_{\text{AMP}\to\text{adenosine via cd73}},\\
\frac{\partial y_4}{\partial t} &= D_5 \Delta\, y_4 + v_3\, y_3/\left(y_3 + k_3\left(1 + y_2/k_i\right)\right) - \underbrace{v_4\, y_4/\left(y_4 + k_4\right)}_{\text{adenosine uptake}},\\
\frac{\partial y_5}{\partial t} &= D_6 \Delta\, y_5 - v_5 y_5 + \mathrm{d}\, n + L_0,
\end{aligned}
\tag{1}
$$

where $n$ is the microglia density, $y_{1,2,3,4}$ are the concentrations of ATP, ADP, AMP and adenosine, respectively. $D_{1,2,3,4,5}$ are the diffusion coefficients and $\chi_{1,2,3,4}$ are the chemotactic motility coefficients. We assume that the

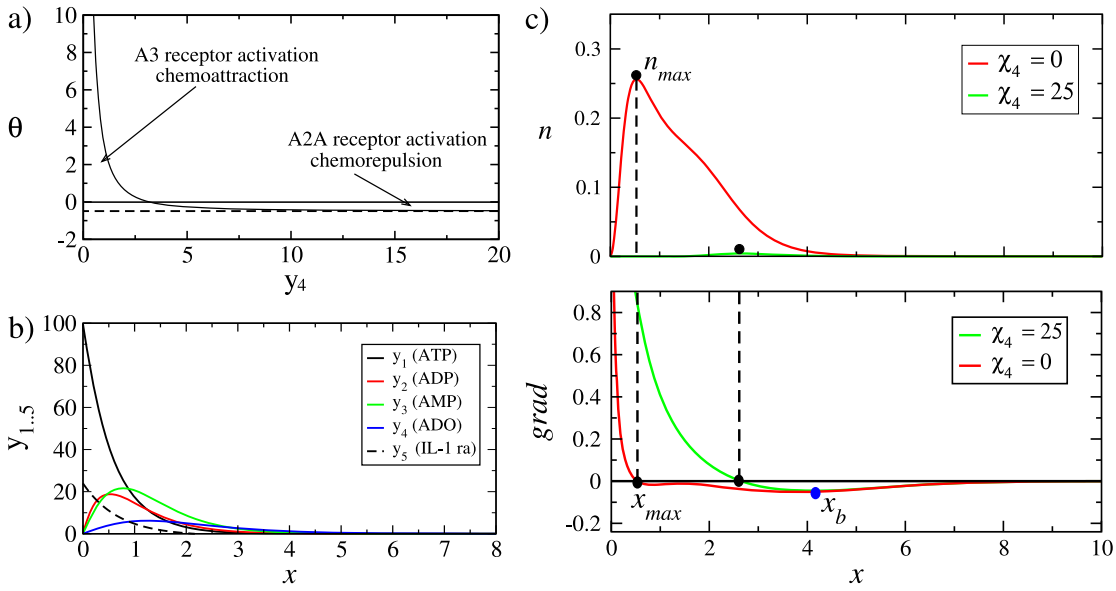


**Figure 2.** (a) The graphical representation of the $\theta(y_4)$ function, which allows us to incorporate the different impact of adenosine on the A3A/A2A receptors for $\gamma = 0.15$ and $\beta = 5$ into model (1); (b) the stationary distributions of ATP and its hydrolysis products together with the stationary distribution of IL-1 antagonist (8). It is assumed that the electrode is located at $x = 0$; (c) the stationary distributions of microglial cells' densities (13), calculated for the different values of chemosensitivity to IL-1 ra $\chi_4$ and corresponding spatial dependences of the total gradient (10). The points of zero-crossing $x_{\max}$ (black filled circles) and global minima $x_b$ (blue filled circles) for the grad($x$) define the location and size of an aggregate. The maximum value of density inside the aggregate is labeled as $n_{\max}$. The values of the other parameters used in the calculations may be found in table 1.

chemotactic sensitivity of microglia to the ATP and ADP is concentration-dependent and is limited by the saturation of the binding process. The saturation of purinergic receptors is described by nonlinear interaction terms in the first equation and prevents the blow-up of a solution, which is observed in the classical Keller–Segel model [58]. The chain of kinetic equations describing the process of hydrolysis ATP ($y_1$) $\rightarrow$ ADP ($y_2$) $\rightarrow$AMP ($y_3$) $\rightarrow$ adenosine ($y_5$) in the ECS [50] is padded by the equation for the concentration of IL-1 ra proteins $y_5$. Here, the maximal rates of the enzymatic reactions are $v_{1,2,3,4}$, $w_1$, and $k_{1,2,3,4}$, $k_i$ are the corresponding Michaelis–Menten constants. The maximal rate of ATP release by microglia is $a$. We use the simplifying assumption that amount of ATP released by the microglial cells is linearly proportional to the number of cells. Another additional source of ATP is the ATP-induced ATP release by reactive astrocytes whose maximal rate equals $b$ [42]. The nonlinear function $\theta(y_4)$ modulating sensitivity of microglia to adenosine is defined as the $\theta(y_4) = (\beta - \gamma y_4^2)/(q_{\text{ado}}^s + y_4^2)$. The specific form of the $\theta$-function was chosen in such a way to take into account the interaction between adenosine and A3A/A2A receptors [27, 34, 54]. In particular, as can be seen from figure 2(a), the nonlinear $\theta$-function takes positive values at moderate concentrations of adenosine in ECS, which means the enhancement of chemotaxis via activation of the adenosine A3A receptors, whereas rather high levels of adenosine cause an activation of A2A receptors which, in turn, leads to substantial retractions of microglial cells and their directed motion towards the electrode. The last equation of the system (1) describes the diffusion of IL-1 ra $y_5$, which spreads away from the coated electrode surface and limits the amount of microglia aggregated around the implantation site. Apparently, the extent to which the IL-1 ra spreads in the ECS depends on the rate of its persistent emission $L_0$ and rate of interaction between microglia cells and IL-1 ra proteins $d$.

## 3. Analytical results for the linearized equations

Let us assume that the total number of microglial cells is fixed and consider the one-dimensional case with no-flux boundary conditions:

$$D_1\frac{\partial n}{\partial x}-\frac{\partial}{\partial x}\left(\frac{\chi_1}{\left(q^s_{\rm atp}+y_1\right)^2}\frac{\partial y_1}{\partial x}+\frac{\chi_2}{\left(q^s_{\rm adp}+y_2\right)^2}\frac{\partial y_2}{\partial x}+\chi_3\,\theta(y_4)\frac{\partial y_4}{\partial x}-\chi_4\frac{\partial y_5}{\partial x}\right)=0,$$
$$\left.\frac{\partial y_i}{\partial x}\right|_{x=0,L}=0, \tag{2}$$

where it is assumed that the electrode is placed at $x=0$ and $L$ is a finite interval or half-plane. We chose asymmetric boundary conditions for the ATP concentration: $y_1(0,\,t)=J_0,\;\; y_1(\infty,\,t)=0$, where $J_0$ is the constant concentration of ATP, which is maintained by the persistent ATP release from microglia and astrocytes at the closest proximity to the electrode surface. Also, it is assumed that the concentration of IL-1 ra near the electrode surface is maintained at the constant level $M_0$. Boundary conditions for ADP, AMP and adenosine are assumed to be zero $y_{2,3,4}(0,\,t)=0,\; y_{2,3,4}(\infty,\,t)=0$. The initial conditions for the cell density and concentrations are $n(0,\,x)=n_0+\epsilon\,\xi(t)$ and $y_i(0,\,x)=y_i^0+\epsilon\,\xi(t)$, where $n_0=0.5$, $x\in[0,\,\infty]$, and $\xi(t)$ is the Gaussian noise of intensity $\epsilon$.

The original model (1) can be non-dimensionalized by means of the following scales:

$$\tilde n=n\,\hat n,\;\; \tilde t=\frac{t}{\tau},\;\tilde x=\frac{x}{\hat x},\;\tau=\frac{1}{\nu_4},\;\; \hat x=\sqrt{D_5\nu_4}, \tag{3}$$

and definitions:

$$\tilde y_1=y_1\frac{(a+b)\hat n}{\left(\nu_1+w_1\right)},\;\; \tilde y_2=y_2\frac{\nu_1\,\hat n}{\nu_2},\;\tilde y_3=y_3\frac{\left(w_1+\nu_2\right)\hat n}{\nu_3},\;\; \tilde y_4=y_4\frac{\nu_3\,\hat n}{\nu_4},\;\; \tilde y_5=y_5\frac{{\rm d}\,\hat n}{\nu_5}, \tag{4}$$

where $\hat n=10^{-3}$ is the equilibrium cell density. The time scale is normalized on a slow rate of adenosine uptake. The dimensionless equations are the following:

$$\frac{\partial n}{\partial t}=D_n\frac{\partial^2 n}{\partial x^2}-\frac{\partial}{\partial x}\left(\frac{n\,A_1}{\left(q^s_{\rm atp}+y_1\right)^2}\frac{\partial y_1}{\partial x}+\frac{n\,A_2}{\left(q^s_{\rm adp}+y_2\right)^2}\frac{\partial y_2}{\partial x}+n\,A_3\,\theta(y_4)\frac{\partial y_4}{\partial x}-n\,A_4\frac{\partial y_5}{\partial x}\right),$$
$$\frac{\partial y_1}{\partial t}=D_{\rm atp}\frac{\partial^2 y_1}{\partial x^2}+C_1\,n+\frac{C_2\,y_1}{y_1+k_b^m}-\frac{C_3\,y_1}{y_1+k_1^m}-\frac{C_4\,y_1}{y_1+k_5^m},$$
$$\frac{\partial y_2}{\partial t}=D_{\rm adp}\frac{\partial^2 y_2}{\partial x^2}+\frac{C_5\,y_1}{y_1+k_1^m}-\frac{C_6\,y_2}{y_2+k_2^m},$$
$$\frac{\partial y_3}{\partial t}=D_{\rm amp}\frac{\partial^2 y_3}{\partial x^2}+\frac{C_7\,y_2}{y_2+k_2^m}+\frac{C_9\,y_1}{y_1+k_5^m}-\frac{C_8\,y_3}{y_3+k_3^m\left(1+y_2/k_i^m\right)},$$
$$\frac{\partial y_4}{\partial t}=\frac{\partial^2 y_4}{\partial x^2}+\frac{C_{10}y_3}{y_3+k_3^m\left(1+y_2/k_i^m\right)}-\frac{C_{11}y_4}{y_4+k_4^m},$$
$$\frac{\partial y_5}{\partial t}=D_{\rm IL1}\frac{\partial^2 y_5}{\partial x^2}-C_{12}y_5+C_{13}n+C_{14},$$
$$D_n=\frac{D_1}{D_5},\;D_{\rm atp}=\frac{D_2}{D_5},\;D_{\rm adp}=\frac{D_3}{D_5},\;D_{\rm amp}=\frac{D_4}{D_5},\;D_{\rm IL1}=\frac{D_6}{D_5}, \tag{5}$$

in this case

$$A_1=\frac{\chi_1(a+b)\hat n}{\left(\nu_1+w_1\right)D_5},\;A_2=\frac{\chi_2\nu_1\,\hat n}{\nu_2\,D_5},\;A_3=\frac{\chi_3\nu_3\,\hat n}{\nu_4\,D_5},\;A_4=\frac{\chi_4\,{\rm d}\,\hat n}{\nu_5\,D_5},$$
$$C_1=\frac{a\left(\nu_1+w_1\right)}{\nu_4\,(a+b)},\;C_2=\frac{\left(\nu_1+w_1\right)b}{\nu_4\,(a+b)},\;C_3=\frac{\left(\nu_1+w_1\right)\nu_1}{\nu_4\,(a+b)\hat n},\;C_4=\frac{\left(\nu_1+w_1\right)w_1}{\nu_4\,(a+b)\hat n},$$
$$C_5=\frac{\nu_2}{\nu_4\hat n},\;C_6=\frac{\nu_2^2}{\nu_1\nu_4\hat n},\;C_7=\frac{\nu_2\nu_3}{\nu_4\left(\nu_2+w_1\right)\hat n},\;C_8=\frac{\nu_3^2}{\nu_4\left(\nu_2+w_1\right)\hat n},\;C_9=\frac{\nu_3 w_1}{\nu_4\left(\nu_2+w_1\right)\hat n},$$

$$C_{10}=\frac{1}{\hat{n}},\ C_{11}=\frac{\nu_4}{\nu_3\hat{n}},\ C_{12}=\frac{\nu_5}{\nu_4},\ C_{13}=\frac{\nu_5}{\nu_4},\ C_{14}=\frac{L_0\ \nu_5}{\nu_4\ d\ \hat{n}},\ k_1^m=\frac{k_1\left(\nu_1+w_1\right)}{(a+b)\hat{n}},$$
$$k_2^m=\frac{k_2\ \nu_2}{\nu_1\hat{n}},\ k_3^m=\frac{k_3\ \nu_3}{\left(\nu_2+w_1\right)\hat{n}},\ k_4^m=\frac{k_4\ \nu_4}{\nu_3\hat{n}},\ k_5^m=\frac{k_5\left(\nu_1+w_1\right)}{(a+b)\hat{n}},\ k_i^m=\frac{k_i\ \nu_2}{\nu_1\hat{n}},\ k_b^m=\frac{k_b\left(\nu_1+w_1\right)}{(a+b)\hat{n}}.$$

The obtained equations (5) can be linearized in the assumption that velocities of diffusive motion near the surfaces of the cells are the same for all chemicals ($D_2=D_3=D_4=D_5=D_6$) and rates of enzymatic reactions $\nu_{1,2,3,4,5}$ are constant and take their maximal values:

$$\frac{\partial n}{\partial t}=D_n\frac{\partial^2 n}{\partial x^2}-\frac{\partial}{\partial x}\left(\frac{n\ A_1}{\left(q_{\rm atp}^s+y_1\right)^2}\frac{\partial y_1}{\partial x}+\frac{n\ A_2}{\left(q_{\rm adp}^s+y_2\right)^2}\frac{\partial y_2}{\partial x}+n\ A_3\theta\left(y_4\right)\frac{\partial y_4}{\partial x}-nA_4\frac{\partial y_5}{\partial x}\right),$$
$$\frac{\partial y_1}{\partial t}=\frac{\partial^2 y_1}{\partial x^2}+B_1 n-B_2 y_1,$$
$$\frac{\partial y_2}{\partial t}=\frac{\partial^2 y_2}{\partial x^2}+B_3 y_1-B_4 y_2,$$
$$\frac{\partial y_3}{\partial t}=\frac{\partial^2 y_3}{\partial x^2}+B_5 y_2+B_6 y_1-B_7 y_3,$$
$$\frac{\partial y_4}{\partial t}=\frac{\partial^2 y_4}{\partial x^2}+B_8 y_3-y_4,$$
$$\frac{\partial y_5}{\partial t}=\frac{\partial^2 y_5}{\partial x^2}-B_9 y_5+B_{10}\ n+B_{11}, \tag{6}$$

where

$$A_1=\frac{\chi_1\left(a+\beta_1\right)\hat{n}}{\left(\nu_1+w_1\right)D_5},\ A_2=\frac{\chi_2\nu_1\hat{n}}{\nu_2 D_5},\ A_3=\frac{\chi_3\nu_3\hat{n}}{\nu_4 D_5},\ A_4=\frac{\chi_4\ \hat{n}L_0}{\nu_5\ D_5},\ B_1=\frac{a\left(\nu_1+w_1\right)}{\nu_4(a+b)},$$
$$B_2=\frac{\left(\nu_1+w_1-b\right)}{\nu_4},\ B_3=\frac{\nu_2(a+b)}{\nu_4\left(\nu_1+w_1\right)},\ B_4=\frac{\nu_2}{\nu_4},\ B_5=\frac{\nu_1\nu_3}{\nu_4\left(\nu_2+w_1\right)},$$
$$B_6=\frac{\nu_3 w_1(a+b)}{\nu_4\left(\nu_2+w_1\right)\left(\nu_1+w_1\right)},\ B_7=\frac{\nu_3}{\nu_4},\ B_8=\frac{\left(\nu_2+w_1\right)}{\nu_3},\ B_9=\frac{\nu_5}{\nu_4},\ B_{10}=\frac{\left(\nu_5+d\right)d}{\nu_4\ L_0},$$
$$B_{11}=\frac{\left(\nu_5+d\right)}{\nu_4}.$$

The studies of the relationship between the chemical signaling and nonlocal interactions of the cells clearly demonstrated that when the chemicals diffuse in the ECS more rapidly than the cells ($D_n\ll 1$), the quasi-stationary spatial distributions of chemicals develop on a faster time scale [43, 55]. The latter means stationarity of the spatial distributions of ATP, ADP, AMP, adenosine and IL-1 ra, which are described by the following steady states equations:

$$\frac{\partial^2 y_1}{\partial x^2}+B_1 n_0-B_2 y_1=0,\ \frac{\partial^2 y_2}{\partial x^2}+B_3 y_1-B_4 y_2=0,\ \frac{\partial^2 y_3}{\partial x^2}+B_5 y_2+B_6 y_1-B_7 y_3=0,$$
$$\frac{\partial^2 y_4}{\partial x^2}+B_8 y_3-y_4=0,\qquad \frac{\partial^2 y_5}{\partial x^2}-B_9 y_5+B_{10} n+B_{11}=0. \tag{7}$$

Linear equations (7) can be solved one by one for the boundary conditions given above in (2). In the one-dimensional case, the quasi-stationary spatial distributions of all chemicals $y_{1,2,3,4,5}$ can be written in the following explicit forms:

$$y_1(x)=J\ {\rm e}^{-\sqrt{B_2}x},\qquad y_2(x)=\frac{J\ B_3}{\left(B_4-B_2\right)}\left({\rm e}^{-\sqrt{B_2}x}-{\rm e}^{-\sqrt{B_4}x}\right),$$

$$y_3(x) = \frac{J\left(e^{-\sqrt{B_2}x} - e^{-\sqrt{B_7}x}\right)}{\left(B_7 - B_2\right)}\left(\frac{B_3B_5}{B_4 - B_2} + B_6\right) - \frac{J\,B_3B_5\left(e^{-\sqrt{B_4}x} - e^{-\sqrt{B_7}x}\right)}{\left(B_4 - B_2\right)\left(B_7 - B_4\right)},$$

$$y_4(x) = -\frac{J\,B_8\left(e^{-\sqrt{B_2}x} - e^{-x}\right)}{\left(B_7 - B_2\right)\left(B_2 - 1\right)}\left(\frac{B_3B_5}{B_4 - B_2} + B_6\right)\frac{J\,B_3B_5B_8\left(e^{-\sqrt{B_4}x} - e^{-x}\right)}{\left(B_4 - B_2\right)\left(B_7 - B_4\right)\left(B_4 - - 1\right)}$$
$$+ \frac{B_8\left(e^{-\sqrt{B_7}x} - e^{-x}\right)}{\left(B_7 - 1\right)}\left[\frac{J}{\left(B_7 - B_2\right)}\left(\frac{B_3B_5}{B_4 - B_2} + B_6\right) - \frac{J\,B_3B_5}{\left(B_4 - B_2\right)\left(B_7 - B_4\right)}\right],$$

$$y_5(x) = M_0\,e^{-\sqrt{B_9}x} + \frac{B_{10}n_0 + B_{11}}{B_9}, \tag{8}$$

where $J = \left(J_0 - B_1n_0/B_2\right)$. These stationary distributions are plotted in figure 2(b).

Given the above expressions for the quasi-stationary distributions (8), the stationary distribution for the density of the microglial cells can be obtained from the equation:

$$K_0 = \frac{\partial}{\partial x}\left(D_n\frac{\partial n}{\partial x} - n\ \mathrm{grad}\,(x)\right), \tag{9}$$

where $K_0$ is the constant, which equals zero due to the no-flux boundary conditions and

$$\mathrm{grad}\,(x) = \frac{n\,A_1}{\left(q^s_{\mathrm{atp}} + y_1\right)^2}\frac{\partial y_1}{\partial x} + \frac{n\,A_2}{\left(q^s_{\mathrm{adp}} + y_2\right)^2}\frac{\partial y_2}{\partial x} + \frac{n\,A_3\left(\beta - \gamma y_4^2\right)}{\left(q^s_{\mathrm{ado}} + y_4\right)^2}\frac{\partial y_4}{\partial x} - nA_4\frac{\partial y_5}{\partial x} \tag{10}$$

is the total gradient, maintaining the motion of microglia towards the source of the inflammation. As follows from the expressions (9) and (10), the density of microglial cells aggregated around the electrode is described by the following equation:

$$\frac{\mathrm{d}n}{\mathrm{d}x} = \frac{n}{D_n}\frac{\mathrm{d}\zeta(x)}{\mathrm{d}x}, \tag{11}$$

where

$$\zeta(x) = -\frac{A_1}{\left(q^s_{\mathrm{atp}} + y_1\right)} - \frac{A_2}{\left(q^s_{\mathrm{adp}} + y_2\right)}$$
$$+ A_3\left(\frac{\left(\gamma\,{q^s_{\mathrm{ado}}}^2 - \beta\right)}{q^s_{\mathrm{ado}} + y_4} + 2\gamma q^s_{\mathrm{ado}}\ln\left(y_4 + q^s_{\mathrm{ado}}\right) - \gamma y_4\right) - A_4\,y_5. \tag{12}$$

The final expression for the cell density can be obtained after integration in (11):

$$n(x) = \exp\left(\zeta(x)/D_n\right). \tag{13}$$

As seen from figure 2(c), the instability of the homogeneous steady state leads to the appearance of an aggregate, the size and spatial location of which are determined by the coordinates of the global minimum and zero-crossing in grad($x$) (10). The physical meaning of the zero-crossing in (10) can be easily understood as a point where the chemoattraction along the total gradient is balanced by the density of the glial scar. As can also be seen from figure 2(c), such zero-crossing points precisely correspond to the coordinates of the maximal values of the density in the formed aggregates. At the same time, the spatial coordinate of the global minimum in grad($x$) might be considered as the point at which the influence of the cells' density overcomes chemoattraction and forms the natural 'backward border' of the aggregate. As follows from the results presented in figure 2(c), the usage of biologically active coat emitting IL-1 ra proteins leads to a drastic reduction of the microglial cells density inside the insulating sheath and shifts it away from the electrode surface. To study the impact of IL-1 ra on the microglia chemotaxis process, we calculated the size and absolute maximal values of the cell density inside the aggregate as functions of the amount of ATP, released from microglia and astrocytes.

As seen from figure 3(a), the spatial location of a global minimum $x_b$ defining the aggregate boundary strongly depends on the rate of the released ATP. At moderate rates of ATP release, the width of the insulating sheath is increased both in the presence of bioactive coating and when IL-1 ra is absent. The increase of the rate of ATP release in the absence of bioactive coating causes the growth and consequent saturation of the microglial cell density inside the aggregate (red solid line in figure 3(c)) as well as the shift of the point $x_{\max}$, where the cell density is maximal, in the direction towards the electrode (red solid line in figure 3(b)). The abrupt shrinkage of

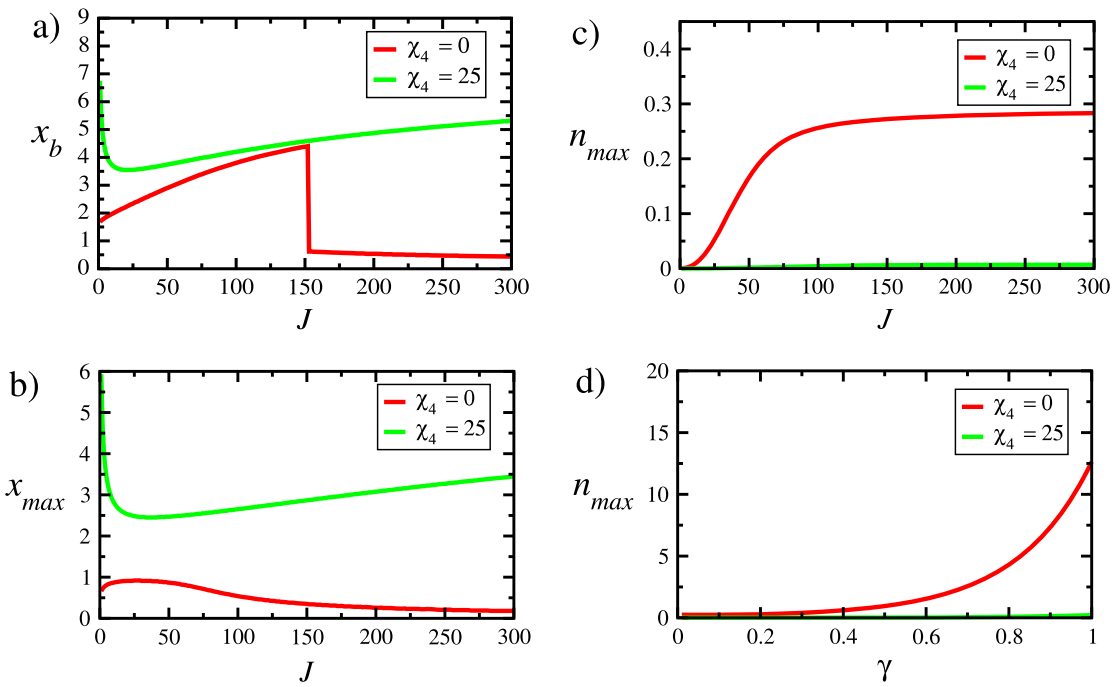


**Figure 3.** The dependences of spatial locations of the global minimum $x_b$ (a) and maximum $x_{max}$ (b) of the gradient (10) on the rate of ATP release. The dependences of the absolute maximal values of the cells density inside the aggregate on the amount of released ATP (c) and on the parameter $\gamma$ regulating the function of adenosine receptors (d). All dependences were calculated for the cases of the absence (red curves) and presence (green curves) of the biologically active coating. The parameters values used in the calculations can be found in table 1.

the sheath at some threshold value of $J$ may be caused by drastic changes in grad($x$) (10), meaning the growth of chemosensitivity with respect to ATP and ADP. The latter effect resembles, to some extent, the enhancement of the immune response, which is observed after the interaction of microglia and laminin [48] and is caused by the ATP-induced vesicle shedding and release of IL-1 cytokine by microglia [59]. In fact, the release of IL-1 cytokine by the microglia in response to the massive release of ATP might mean the appearance of another substance, playing the role of a chemo-attractant. It becomes clear in this context that the IL-1 ra electrode coating allows to weaken that part of the chemotactic signaling process, which is related to the ATP-induced release of IL-1 cytokine [59].

The application of the IL-1 ra coating causes qualitative changes in the tissue response to the growing level of extracellular ATP. In particular, the presence of bioactive coating weakens the additional chemo-attraction induced by the released IL-1 cytokines and prevents the shrinkage of the insulating sheath (green curve in figure 3(a)). Moreover, the presence of IL-1 ra induces strong reduction of microglial cell density inside the aggregate (green curve in figures 3(c)) and prevents its movement in the direction towards the electrode surface even for high levels of ATP release (green curve in figures 3(b)). Another important parameter affecting the process of microglia chemotaxis is $\gamma$, which is responsible for the functional regulation of adenosine A3A/A2A receptors. The substantial increase of the microglia cell density is observed for rather large values of $\gamma$ in the absence of bioactive coating (see the red curve in figure 3(d)). This fact can be explained by the enhanced retractions of microglial cells which react this way to the increase of adenosine levels in the ECS. As shown in figure 3(d), the presence of IL-1 ra compensates the growth of the cell density caused by the increased level of extracellular adenosine. Dependences similar to those presented in figure 3 can be reproduced in a wide range of the values of parameters shown in table 1.

To study the role played by the parameters, characterizing the bioactive coating, on the aggregation process, we calculated the microglial cell density (13) for different values of the chemosensitivity coefficient $\chi_4$ as well as for the different values of IL-1 ra a concentrations $M_0$. As illustrated in figure 4, these two parameters have a similar effect on the cell density, namely, both a substantial increase of chemotactic sensitivity to IL-1 ra (see figure 4(a)) and a high concentration of IL-1 ra near the electrode surface lead to a strong reduction of the aggregate and limit the spread of inflammatory factors.

**Table 1.** Description and values of parameters used in simulations.

| Parameter | Description | Value | Reference |
|---|---|---|---|
| $D_1$ | Random motility of microglial cells | $3\,\frac{\mu m^2}{min}$ | [47] |
| $D_{2,3,4,5,6}$ | Diffusion coefficients for ATP, ADP, adenosine, IL-1 ra | $100\,\frac{\mu m^2}{min}$ | [47] |
| $\nu_1$ | Rate of ATP to ADP conversion by ATPase | $17\ min^{-1}$ | [50] |
| $\nu_2$ | Rate of ADP to AMP conversion by ADPase | $10\ min^{-1}$ | [50] |
| $w_1$ | Rate of ATP to AMP conversion by cd39 | $0.16\ min^{-1}$ | [46] |
| $\nu_3$ | Rate of AMP to adenosine conversion by cd73 | $15\ min^{-1}$ | [50] |
| $\nu_4$ | Rate of adenosine uptake | $2.36\ min^{-1}$ | [50] |
| $\chi_1$ | Chemosensitivity of microglia to ATP | $6\,\frac{\mu\ m^2}{\mu M\ min}$ | [47] |
| $\chi_2$ | Chemosensitivity of microglia to ADP | $6\,\frac{\mu\ m^2}{\mu M\ min}$ | [47] |
| $\chi_3$ | Chemoattraction/chemorepulsion of adenosine | $1\,\frac{\mu m^2}{\mu\ M\ min}$ | [34] |
| $a$ | Rate of ATP production by microglial cells | $10\ min^{-1}$ | [50] |
| $b$ | Rate of ATP production by astrocytes | $10\ min^{-1}$ | [51] |
| $k_1$ | Reaction constant for ATPase | $5\ \mu M$ | [57] |
| $k_2$ | Reaction constant for ADPase | $1.5\ \mu M$ | [57] |
| $k_3$ | Reaction constant for cd73 | $1\ \mu M$ | [57] |
| $k_4$ | Reaction constant for adenosine degradation | $0.22\ \mu M$ | [57] |
| $k_5$ | Reaction constant for cd39 | $0.22\ \mu M$ | [57] |
| $k_i$ | Reaction constant for AMP degradation | $1.0\ \mu M$ | [57] |
| $k_b$ | Reaction constant for ATP release | $2.0\ \mu M$ | [57] |
| $d$ | Uptake rate constant for IL-1 ra | $0.5\ min^{-1}$ | |
| $q^s_{atp}$, $q^s_{adp}$ | Binding constants for ATP and ADP | $2.2\ min^{-1}$ | |
| $q^s_{ado}$ | Binding constant for adenosine | $1.57\ min^{-1}$ | |
| $J_0$ | Rate of ATP release near the electrode surface | $100\ min^{-1}$ | |
| $L_0$ | Rate of IL-1 ra emission near the electrode surface | $1\ min^{-1}$ | |
| $M_0$ | Concentration of IL-1 ra near the electrode surface | $25\ min^{-1}$ | |

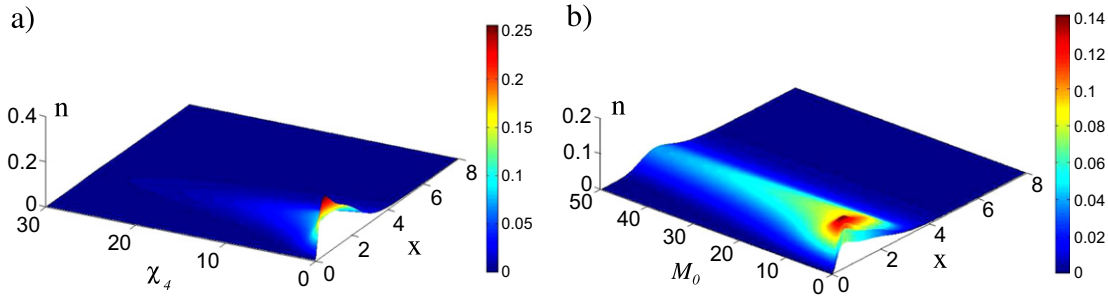


**Figure 4.** The spatial dependences of microglial cells' density (13) calculated (a) for the different values of coefficient $\chi_4$ and (b) for the different values of concentration of IL-1 ra on the electrode surface $M_0$. The value of the coefficient $\chi_4 = 5$ is fixed in (b).

## 4. Stability of homogeneous steady state and impact of bioactive coating

To study the impact of the bioactive coating in terms of stability theory, we linearized the equations (6) about the homogeneous steady state $(\hat{n}, \hat{y}_1, \hat{y}_2, \hat{y}_3, \hat{y}_4, \hat{y}_5)$ and reduced our stability analysis to the solution of eigenvalue problem. For the one-dimensional spatial domain of length $L$ with no-flux boundary conditions, the eigenfunctions are of the form $\Phi_n(x) = \exp(j\ kx)$, and the eigenvalues are $k_n^2 = \pi^2 n^2 / L^2$, where $k = \pi n / L$ is the wavenumber and the positive integer $n$ is the mode number. Let us consider small perturbations of the steady state of the form:

$$\left(\hat{n}, \hat{y}_1, \hat{y}_2, \hat{y}_3, \hat{y}_4, \hat{y}_5\right)(x, t) = \left(n^0, y_1^0, y_2^0, y_3^0, y_4^0, y_5^0\right) \exp(\lambda t + j\ kx). \quad (14)$$

A substitution of the equations (14) into (6) and linearization of the obtained system of equations allowed us to get the Jacobian matrix:

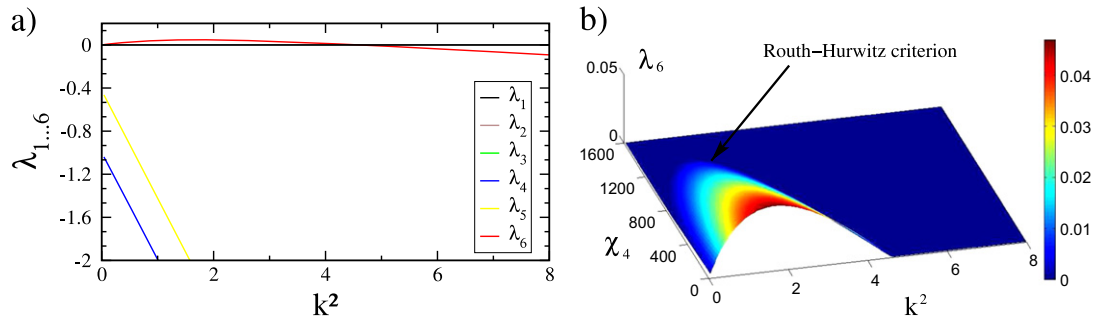


**Figure 5.** (a) The dispersion curves calculated from the (15) for the values of parameters presented in table 1 and $\chi_4 = 0$; (b) the dispersion curves $\lambda_6(k^2)$, calculated for the different values of $\chi_4$. The borders of the area of spatial instability (black solid line) were calculated by means of the Routh–Hurwitz criterion.

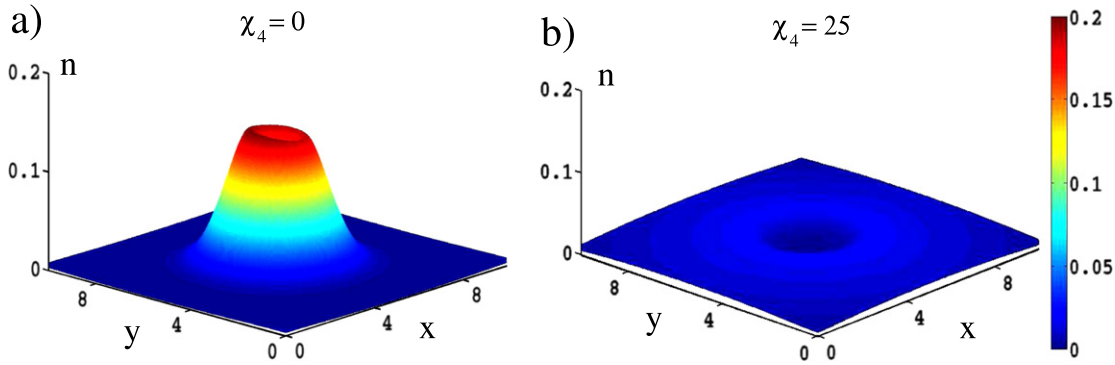


**Figure 6.** The normalized two-dimensional spatial distributions of microglial cell density calculated for the model equations (5) in the absence (a) and in the presence (b) of bioactive coating. The rate of ATP release is $J = 100$ and $\gamma = 0.15$. The values of the other parameters can be found in table 1. The size of the square domain around the electrode is $10 \times 10$ in arbitrary units. The total time of the numerical integration is $T = 100$. The chosen spatial scale is $\Delta x = 0.033$.

$$A\left(k^2\right) = \begin{bmatrix} -k^2 D_n & n_0 A_1 k^2 & n_0 A_2 k^2 & 0 & -n_0 A_3 \gamma_0 k^2 & -A_4 k^2 n_0 \\ B_1 & -k^2 - B_2 & 0 & 0 & 0 & 0 \\ 0 & B_3 & -k^2 - B_4 & 0 & 0 & 0 \\ 0 & B_6 & B_5 & -k^2 - B_7 & 0 & 0 \\ 0 & 0 & 0 & B_8 & -k^2 - 1 & 0 \\ B_{10} & 0 & 0 & 0 & 0 & -k^2 - B_9 \end{bmatrix}$$

and the determinant $\det(\lambda - A(k^2)I)$ to obtain the sixth-order characteristic equation:

$$a_1\left(k^2\right)\lambda^6 + a_2\left(k^2\right)\lambda^5 + a_3\left(k^2\right)\lambda^4 + a_4\left(k^2\right)\lambda^3 + a_5\left(k^2\right)\lambda^2 + a_6\left(k^2\right)\lambda + a_7\left(k^2\right) = 0, \qquad (15)$$

whose roots $\lambda_{1..6}$ define the domain of spatial instability for the homogeneous steady state. The dependences $\lambda_{1..6}(k^2)$ are calculated for a particular range of values of the control parameters (figure 4(a)). Obviously, five eigenvalues take negative values for all wavenumbers. Thus, the spatial stability of the homogeneous steady state depends on the sign of $\lambda_6$ and is defined by the dispersion curve $\lambda_6(k^2)$ as shown in figure 5(a). To reveal the impact of the bioactive coating on the spatial stability of the homogeneous steady state, we calculated the dispersion curves $\lambda_6(k^2)$ for different values of the chemosensitivity $\chi_4$. As follows from the results presented in figure 5(b), an increase of the chemosensitivity to the IL-1 ra leads to a substantial decrease of the area of instability where $\lambda_6$ takes positive values. Moreover, the analysis of the roots of the characteristic equation (15) by means of the Routh–Hurwitz theory allowed us to estimate the boundaries of the domain of the spatial instability. The results of this analysis are in good agreement with the results of the direct numerical solution of equation (15). As illustrated in figure 5(b), the area of instability is finite, localized in space near the electrode and decreases as the coefficient of chemosensitivity to the IL-1 ra $\chi_4$ increases. Also the absolute values of $\lambda_6$ decrease in the presence of the IL-1 antagonist, what may be interpreted as a reduction of the instability caused by the

release of ATP in ECS. These last findings are in good agreement with the analytical results presented above concerning the impact of the bioactive coating on the size and location of the glial sheath. Indeed, as seen from the results presented above in figure 2(c), the use of the bioactive coating leads to a substantial decrease of the cell density inside the aggregate as well as its removal from the electrode.

## 5. Results of numerical simulations

To verify the analytical results obtained for the original nonlinear model, we performed numerical integrations of the dimensionless equations (5) for the two-dimensional case by using the standard finite-difference scheme together with the high order explicit method for stiff differential equations utilizing the explicit Runge–Kutta–Chebyshev formulas [52]. The choice of the two-dimensional geometry may simplify the comparison of the obtained numerical results and results of representative microscopy (X10) data of horizontal brain sections immunostained for GFAP surrounding the electrode insertion site, which are presented in [49]. We assumed that the electrode is located in the center of the square domain which allows us to model the realistic situation, when it is symmetrically enwrapped by the microglial cells. The obtained values of the cell density were normalized by the total density inside the chosen domain, which is calculated as a sum of all values of $n$, calculated in each point on the equidistant grid. Since the expressions for $A_1$, $A_2$, $A_3$ are different for the systems (5) and (6), then for the numerical integration of the system (5) the absolute values of chemosensitivity coefficients were chosen equal to $\chi_5 = 5 \times 10^{-5}$, $\chi_2 = 5 \times 10^{-5}$, $\chi_3 = 1 \times 10^{-5}$, respectively.

As shown in figure 5, the emission of IL-1 ra proteins by the anti-inflammatory coating leads to a drastic reduction of the cell density around the electrode and nearly prevents the scarring process. The two-dimensional stationary spatial distributions of ATP, ADP and adenosine have similar profiles to those obtained in the one-dimensional case shown in figure 2(b). These findings are in good qualitative agreement with recent experimental results [49]. In particular, the two-dimensional plots in figure 6 resemble the results of representative microscopy (X10) data of horizontal brain sections, which can be found in [49]. As already discussed in section 3, the strategy of the suppression of the acute immune response aims to eliminate the chemotactic signaling which is related to the release of IL-1 cytokines and may be considered as a very effective approach to prevent scar formation. Moreover, the suppression of the cytokine release may play a crucial role in the prevention of astrogliosis responsible for substantial decrease of the extracellular volume. The shrinkage of extracellular volume is known to induce the appearance of diffusive barriers in the ECS which are able to affect the diffusion of molecules and limit the spread of the chemotactic signaling to the closest proximity of the electrode [60].

## 6. Conclusions

We presented a simple mathematical model of the acute chemotactic response of the microglia to the electrode implantation, which is accompanied by a massive release of ATP. Given the recent experimental results, we assumed that the chemotactic signaling and motility of microglia are maintained by the chain of enzymes' reactions on the surfaces of microglial cells, which performs the hydrolysis of ATP to adenosine. Based on our model, we found that the release of a substantial amount of ATP into the ECS induces the chemotactic motion of microglia towards the electrode. The stationary spatial distributions of ATP and its hydrolysis products together with the stationary distribution of microglial cell density were calculated analytically for the one-dimensional case. We also demonstrated the possibility of an abrupt shrinkage of the insulating sheath for some threshold values of ATP concentration.

With our model, we analyzed possible effects of anti-inflammatory bioactive coating on the glial scarring process. In particular, we found that a recently proposed bioactive coating shifts the emerging encapsulating sheath away from the electrode, preventing its abrupt shrinkage and stabilizing the cell density around the electrode at a moderate level. Thus, the usage of the anti-inflammatory bioactive coating containing the proteins of the IL-1 antagonist, is able to suppress or significantly diminish the scarring process around the implantation site which, in turn, can increase the conductance and signal-to-noise ratio of the electrode–tissue interface.

## References

[1] Nicolelis M A L *et al* 2003 Chronic, multisite, multielectrode recordings in macaque monkeys *Proc. Natl Acad. Sci. USA* **100** 11041–6
[2] Carmena J M *et al* 2003 Learning to control a brain–machine interface for reaching and grasping by primates *PLoS Biol.* **1** 193–208
[3] Deutschl G *et al* 2006 A randomized trial of deep-brain stimulation for Parkinson's disease *New England J. Med.* **355** 896–908
[4] Tass P, Qin L, Hauptmann C, Dovero S, Bezard E, Boraud T and Meissner W G 2012 Coordinated reset has sustained aftereffects in Parkinsonian monkeys *Ann. Neurology* **72** 816–20
[5] Hochberg L R *et al* 2006 Neuronal ensemble control of prosthetic devices by a human with tetraplegia *Nature* **442** 164–71

[6] Wessberg J *et al* 2000 Real-time prediction of hand trajectory by ensembles of cortical neurons in primates *Nature* **408** 361–5
[7] Schwartz A B, Cui X T, Weber D J and Moran D W 2006 Brain-controlled interfaces: movement restoration with neural prosthetics *Neuron* **52** 205–20
[8] Polikov V S, Tresco P A and Reichert W M 2005 Response of brain tissue to chronically implanted neural electrodes *J. Neurosci. Methods* **148** 1–18
[9] Polikov V S, Block M L, Fellous J M, Hong J S and Reichert W M 2006 *In vitro* model of glial scarring around neuroelectrodes chronically implanted in the CNS *Biomaterials* **27** 5368–76
[10] Szarowski D H *et al* 2003 Brain responses to micro-machined silicon devices *Brain Res.* **983** 23–35
[11] Kim Y T, Hitchcock R W, Bridge M J and Tresco P A 2004 Chronic response of adult rat brain tissue to implants anchored to the skull *Biomaterials* **25** 2229–37
[12] McConnell G C, Butera1 R J and Bellamkonda R V 2009 Bioimpedance modeling to monitor astrocytic response to chronically implanted electrodes *J. Neural Eng.* **6** 055005
[13] McConnell G C, Rees H D, Levey A I, Gutekunst C, Gross R E and Bellamkonda R V 2009 Implanted neural electrodes cause chronic, local inflammation that is correlated with local neurodegeneration *J. Neural Eng.* **6** 056003
[14] Butson C R and McIntyre C C 2005 Tissue and electrode capacitance reduce neural activation volumes during deep brain stimulation *Clin. Neurophysiol.* **116** 2490–500
[15] Butson C R, Maks C B and McIntyre C C 2006 Sources and effects of electrode impedance during deep brain stimulation *Clin. Neurophysiol.* **117** 447–54
[16] Lempka S F, Miocinovic S, Johnson M D, Vitek J L and McIntyre C C 2009 *In vivo* impedance spectroscopy of deep brain stimulation electrodes *J. Neural Eng.* **6** 046001–11
[17] Miocinovic S, Lempka S F, Russo G S, Maks C B, Butson C R, Sakaie K E, Vitek J L and McIntyre C C 2009 Experimental and theoretical characterization of the voltage distribution generated by deep brain stimulation *Exp. Neurology* **216** 166–76
[18] Wider C, Pollo C, Bloch J, Burkhard P R and Vingerhoets F J G 2008 Long-term outcome of 50 consecutive Parkinsons disease patients treated with subthalamic deep brain stimulation *Parkinsonism Rel. Disord.* **14** 114–9
[19] Chabot S, Williams G and Yong V W 1997 Microglial production of TNF-alpha is induced by activated T lymphocytes involvement of VLA-4 and inhibition by interferonbeta-1 b *J. Clin. Invest.* **100** 604–12
[20] Giulian D, Li J, Leara B and Keenen C 1994 Phagocytic microglia release cytokines and cytotoxins that regulate the survival of astrocytes and neurons in culture *Neurochem. Int.* **25** 227–33
[21] Grill W M and Mortimer J T 1994 Electrical properties of implant encapsulation tissue *Ann. Biomed. Eng.* **22** 23–33
[22] Lempka S F and McIntyre C C 2013 Theoretical analysis of the local field potential in deep brain stimulation applications *PLoS One* **8** e59839
[23] Chu K T *et al* 2012 Inhibition of P2X7 receptor ameliorates transient global cerebral ischemia/reperfusion injury via modulating inflammatory responses in the rat hippocampus *J. Neuroinflamm.* **9** 69
[24] Ferrari D *et al* 2006 The P2X(7) receptor: A key player in IL-1 processing and release *J. Immunology* **176** 3877–83
[25] Kronlage M *et al* 2010 Autocrine purinergic receptor signaling is essential for macrophage chemotaxis *Sci. Signal* **3** ra55
[26] Lee K H, Chang S Y, Roberts D W and Kim U 2004 Neurotransmitter release from high-frequency stimulation of the subthalamic nucleus *J. Neurosurg.* **101** 511–7
[27] Junger W G 2011 *Nat. Rev. Immunology* **11** 201–12
[28] Ohsawa K and Kohsaka S 2011 Dynamic motility of microglia: purinergic modulation of microglial movement in the normal and pathological brain *Glia* **59** 1793–9
[29] Davalos D *et al* 2005 ATP mediates rapid microglial response to local brain injury *in vivo Nat. Neurosci.* **8** 752–8
[30] Dou Y *et al* 2012 Microglial migration mediated by ATP-induced ATP release from lysosomes *Cell Res.* **22** 1022–33
[31] Imura Y *et al* 2013 Microglia release ATP by exocytosis *Glia* **61** 3120–30
[32] Silchenko A N and Tass P 2008 Computational modeling of paroxysmal depolarization shifts in neurons induced by the glutamate release from astrocytes *Biol. Cybern.* A **98** 61–74
[33] Honda S *et al* 2001 Extracellular ATP or ADP induce chemotaxis of cultured microglia through G(i/o)-coupled P2Y receptors *J. Neurosci.* **21** 1975–82
[34] Orr A G, Orr A L, Li X J, Gross R E and Traynelis S F 2009 Adenosine A(2A) receptor mediates microglial process retraction *Nat. Neurosci.* **12** 872–8
[35] Faerber K *et al* 2008 The ectonucleotidase cd39/ENTPDase1 modulates purinergic-mediated microglial migration *Glia* **56** 331–41
[36] Haynes S E *et al* 2006 The P2Y(12) receptor regulates microglial activation by extracellular nucleotides *Nat. Neurosci.* **9** 1512–9
[37] Chen Y *et al* 2006 ATP release guides neutrophil chemotaxis via P2Y2 and A3 receptors *Science* **314** 1792–5
[38] Antonioli L, Pacher P, Vizi E S and Hasko G 2013 cd39 and cd73 in immunity and inflammation *Trends Mol. Med.* **9** 355–67
[39] Keller E F and Segel L A 1970 Initiation of slime mold aggregation viewed as instability *J. Theor. Biol.* **26** 399–415
[40] Othmer H G and Stevens A 1997 Aggregation, blowup, and collapse: the ABC's of taxis in reinforced random walks *SIAM J. Appl. Math.* **57** 1044–81
[41] Hillen T and Painter K 2001 Global existence for a parabolic chemotaxis model with prevention of overcrowding *Adv. Appl. Math.* **26** 280–301
[42] Kettenmann H and Ransom B R 1995 *Neuroglia* (Oxford: Oxford University Press) 60–71
[43] Luca M, Chavez-Ross A, Edelstein-Keshet L and Mogilner A 2003 Chemotactic signaling, microglia, and Alzheimer's disease senile plaques: is there a connection? *Bull. Math. Biol.* **65** 693–730
[44] Penner K, Ermentrout B and Swigon D 2012 Pattern formation in a model of acute inflammation *SIAM J. Appl. Dyn. Sys.* **11** 629–60
[45] Corriden R and Insel P A 2012 New insights regarding the regulation of chemotaxis by nucleotides, adenosine, and their receptors *Purinergic Signalling* **8** 587–98
[46] Bennett M R, Farnell L and Gibson W G 2009 P2X(7) regenerative-loop potentiation of glutamate synaptic transmission by microglia and astrocytes *J. Theor. Biol.* **261** 1–16
[47] Moghe P V, Nelson R D and Tranquillo R T 1995 Cytokine-stimulated chemotaxis of human neutrophils in a 3D conjoined fibrin gel assy *J. Immunology Methods* **180** 193–211
[48] He W, McConnell G C and Bellamkonda R V 2006 Nanoscale laminin coating modulates cortical scarring response around implanted silicon microelectrode arrays *J. Neural Eng.* **3** 316–26
[49] Taub A H, Hogri R, Magal A, Mintz M and Shacham-Diamand Y 2012 Bioactive anti-inflammatory coating for chronic neural electrodes *J. Biomed. Mater. Res.* A **100A** 1854–58

[50] Gordon E L, Pearson J D and Slakey L 1995 The hydrolysis of extracellular adenine-nucleosides by cultured endothelial-cells from pig aorta—feedforward inhibition of adenosine production at the cell surface *Biol. Chem.* **261** 5496–504
[51] Anderson C M, Bergher J P and Swanson R A 2004 ATP-induced ATP release from astrocytes *J. Neurochem.* **88** 246–56
[52] Medovikov A A 1998 High order explicit methods for parabolic equations *BIT* **38** 372–90
[53] Schaaf R 1985 Stationary solutions of chemotaxis systems *Trans. Am. Math. Soc.* **292** 531–56
[54] Silchenko A N and Tass P 2013 Computational modeling of chemotactic signaling and aggregation of microglia around implantation site during deep brain stimulation *Eur. Phys. J.—Spec. Top.* **222** 2647–53
[55] Lee C, Hoopes M, Diehl J, Gilliland W, Huxel G, Leaver E V, McCann K, Umbanhowar J and Mogilner A 2001 Non-local concepts and models in biology *J. Theor. Biol.* **210** 201–19
[56] Zimmermann H 2006 Ectonucleotidases in the nervous system *Novartis Found. Symp.* **276** 113–28
[57] Meghji P, Pearson J D and Slakey L L 1995 Kinetics of extracellular ATP hydrolysis by microvascular endothelial cells from rat heart *Biochem. J.* **308** 725–31
[58] Painter K J and Hillen T 2002 Volume-filling and quorum-sensing models for chemosensitive movement *Can. Appl. Math. Q.* **10** 501–43
[59] Bianco F, Pravettoni E, Colombo A, Schenk U, Moller T, Matteoli M and Verderio C 2005 Astrocyte-derived ATP induces vesicle shedding and IL-1 beta release from microglia *J. Immunology* **174** 7268–77
[60] Roitbak T and Sykova E 1999 Diffusion barriers evoked in the rat cortex by reactive astrogliosis *Glia* **28** 40–48